Reconstruction of plasma density profiles by measuring spectra of radiation emitted from oscillating plasma dipoles

S Kylychbekov[1,4]**, H S Song**[1,4]**, K B Kwon**[1]**, O Ra**[1]**, E S Yoon**[1]**, M Chung**[1]**, K Yu**[2]**, S R Yoffe**[3]**, B Ersfeld**[3]**, D A Jaroszynski**[3] **and M S Hur**[1]

[1] UNIST, Unist-gil 50, Ulsan, 44919 Republic of Korea
[2] Computational Science Initiative, Brookhaven National Laboratory, Upton, New York 11973, United States of America
[3] Department of Physics, SUPA and University of Strathclyde, Glasgow, G40NG, United Kingdom

E-mail: mshur@unist.ac.kr

Abstract

We suggest a new method for characterising non-uniform density distributions of plasma by measuring the spectra of radiation emitted from a localised plasma dipole oscillator excited by colliding electromagnetic pulses. The density distribution can be determined by scanning the collision point in space. Two-dimensional particle-in-cell simulations demonstrate the reconstruction of linear and nonlinear density profiles corresponding to laser-produced plasma. The method can be applied to a wide range of plasma, including fusion and low temperature plasmas. It overcomes many of the disadvantages of existing methods that only yield average densities along the path of probe pulses, such as interferometry and spectroscopy.

Keywords: plasma diagnostics, plasma dipole oscillation, point-detect of plasma density, density scanning, radiation emission from plasma, plasma dipole radiation

Introduction

Characterization of plasma parameters [1] is critical for accurately interpreting its behaviour, control and confinement. One of the most important parameters to be measured is the density of charge carriers (i.e. electrons), which is pertinent to almost all plasma phenomena, from general collective behaviour to its electrical and optical characteristics. Furthermore, quantitative knowledge of the electron density, its fluctuation and profile type is required for developing fusion plasma devices [2–10] and for understanding laser-plasma interactions in general [11–14]. It is also necessary for characterising plasma-related instruments, including those used for material processing [15–19]. Many plasma diagnostics techniques currently exist; their operating principles depend on the plasma parameter regimes. Research into new diagnostic methods is always ongoing, especially for use under the harsh conditions of fusion plasma and laser-plasma interactions.

The most widely used and well-developed plasma diagnostics technique is interferometry, which exploits the change in phase that electromagnetic (EM) waves experience as they pass through media with variable refractive indices. By analysing the resulting interference fringes using mathematical inversion processes, such as the Abel inversion, the plasma density can be deduced [1, 4, 12, 15, 16]. However, the technique has limitations: the phase change is integrated along the path, and the local density cannot be determined at specific points along them unless particular symmetries are assumed. Tomographic methods are useful in deducing the density distribution by applying inversion algorithms to significant amount of data from many data acquisition channels, but are not suitable for measuring the local density at desired positions [19]. In contrast, reflectometry is designed to

[4] These two authors equally contributed to this study as co-first-authors.

measure the local electron density [6–10] and is often used for fluctuation analysis and edge plasma density probing. However, to reconstruct the plasma density profile a wide range of EM frequencies from sources, that are not usually widely available, are required. Electrical or Langmuir probes [20–23] are widely used for local density characterization, but they are necessarily invasive. Furthermore, they cannot be used to measure laser-plasma systems because of the tiny volumes that their plasma features occupy, i.e. smaller than a few millimetres [11–14]. Collective Thomson scattering techniques are appropriate tools for fluctuation analysis, but not for measuring density profiles or densities at a specific point [24, 25]. The polarimetry technique gives the line-integrated information of the magnetic field and density but not the local plasma density [26].

Raman spectroscopy is commonly used for measuring the density of high-density plasma, such as from laser-matter interactions: the difference between the probe frequency and its Stokes (or anti-Stokes) is used to determine the plasma density. Methods of simultaneous measurement of the plasma density and temperature or the magnetic field, utilizing the different characteristics between the forward- and backward-Raman scatter, have been studied [27–29]. As for inter-ferometry, spectroscopy is limited to the line-integral of the density along the path of the probe pulse. However, the phase analysis of chirped Raman backscattered radiation can be used to reconstruct non-uniform density profiles [14]. Stark broadening has also been used to measure the density and temperature of plasma, but its resolution depends on imaging systems that have a small confocal parameter [30].

In this work, we report a novel way of measuring the local electron density of plasma, which can be used to reconstruct non-uniform density profiles. The method exploits the radiation produced by an induced local plasma dipole oscillation (PDO), which emits at the local plasma frequency. The plasma density can be deduced from measurements of the frequency of the PDO radiation. A key challenge is how to generate a local PDO.

We recently reported a new way of generating PDOs [31, 32]. Two counter-propagating laser pulses, with slightly detuned wavelengths, are fired into plasma to overlap at a desired position, where they generate a moving ponderomotive (PM) potential train with a phase velocity proportional to the detuning. The PM potential associated with the beat-wave drags the electrons over the background ions until the attractive force exerted by the ions exceeds the PM potential threshold. This produces a stationary plasma dipole. Subsequently, as the PM potential diminishes, the dragged plasma dipole is released and starts to oscillate at the local plasma frequency. The oscillating electric dipole generates radiation with a quasi-narrowband peak at the plasma frequency $\omega_p \propto \sqrt{n}$, where n is the local electron density surrounding the induced dipole. Hence, the plasma density can be determined by measuring the radiation frequency. Scanning the collision position of the laser pulses, e.g. by changing their angles or relative time delays, enables reconstruction of the density profile. One limitation is that the method cannot be used directly to determine non-monotonic

density distributions, as will be further discussed below. We demonstrate, using two-dimensional (2D) particle-in-cell (PIC) simulations, how the suggested method can be used to reconstruct linear and nonlinear density profiles with a range of different slopes. For a non-monotonic density profile, the monotonic parts can be reconstructed precisely, but the measurement of density in a trough is prone to uncertainty, which we discuss further below.

The paper is organized as follows. First, we present the theoretical background and analyse the dipole formation using 1D simulations. We then demonstrate the results of plasma diagnostic simulations using 2D PIC simulations. In the final section we discuss applications of the method to different types of plasma and discuss the modification of the dipole oscillation in thermal plasma.

Overview

The principle of the method involves two stages that should be analysed in sequence. In the first stage, a dipole of electrons is induced in plasma by the ponderomotive force of colliding laser pulses. The second stage involves emission of radiation from the excited dipole and detecting it for diagnostic purposes. For the simulations, we use the PIC code, cplPIC, which has been verified through numerous simulation studies [27, 28, 31–35].

Formation of an isolated plasma dipole oscillation

In this section we describe the formation of a localized PDO, which is illustrated using 1D PIC simulations. For simplicity, we consider cold and non-magnetized plasma, in which an electron's response to the laser field is much faster than thermal or cyclotron motion. Ions are considered immobile on the time scale of the fast motion of electrons. The plasma is considered preformed and quasi-neutral, with a density giving a plasma frequency of 10–20 THz. However, the method can be readily extended to other densities. As an example we consider two short duration (a few tens of femtoseconds), counter-propagating, weakly-relativistic laser pulses with $a_0 = 0.1 - 0.3$, where the normalised laser amplitude $a_0 = eE_0/(mc\omega)$, E_0 and ω are the peak electric field strength and the frequency of the laser pulses, respectively, e and m are the electron unit charge and mass, and c the speed of light in vacuum. The laser pulses, with wavelengths 800 and 790 nm, approximately detuned by ω_p, are made to overlap at a desired position in the plasma.

A slowly-moving ponderomotive (PM) beat potential is generated in the region where the laser pulses overlap

$$\phi_{\text{PM}} = 2a_0^2 e^{-\left(\frac{(z/c-t)^2}{\tau^2} + \frac{(z/c+t)^2}{\tau^2}\right)} \cos((k_1 + k_2)z$$
$$- (\omega_1 - \omega_2)t), \tag{1}$$

where k_i and ω_i are, respectively, the wave numbers and frequencies of the lasers ($i = 1, 2$). The beat potential moves
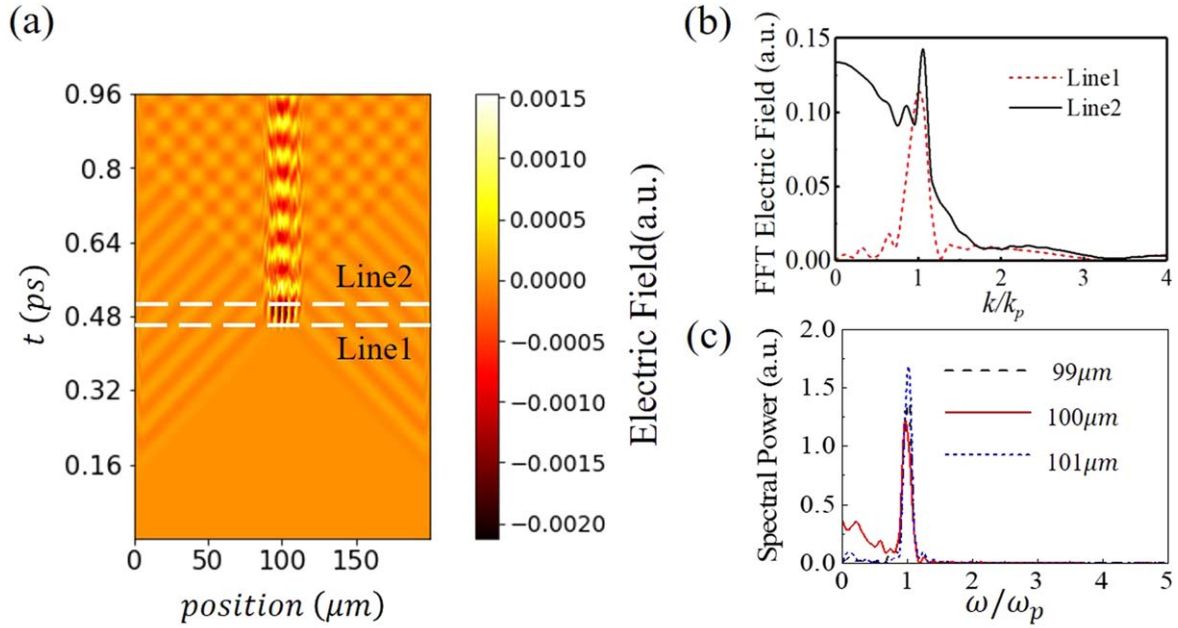
Figure 1. Build-up process of the dipole field in a plasma. (a) Density plot of the longitudinal (x) electric field in $t-x$ domain as the laser pulses propagate in $+x$ and $-x$ directions. The dipole field is induced over 0.02 ps at ~ 0.48 ps, between lines 1 and 2. (b) Fast Fourier transforms (FFTs) along lines 1 and 2. Wave number is normalized by plasma wave number $\boldsymbol{k_p} = \boldsymbol{\omega}/\boldsymbol{c}$. Just before the generation of the dipole field (along line 1), only the wake field exists; its spatial spectrum has a strong peak at $\boldsymbol{k_p}$. After generation of the dipole field, the $\boldsymbol{k} = 0$ mode (i.e. in-phase motion) becomes dominant. (c) FFT of the temporal evolution of the fields measured at different positions inside the dipole between 99 and 101 μm. Frequency is normalized to the plasma frequency $\boldsymbol{\omega_p}$. All the spectra peak at the plasma frequency.

at phase velocity

$$v_\phi = \frac{\omega_1 - \omega_2}{k_1 + k_2} \ll c. \qquad (2)$$

Electrons, driven by the beat PM force, form a plasma wave that grows until it reaches the wave-breaking limit, which occurs in a few cycles of oscillation. The electrons are subsequently trapped in the PM potential troughs to form a train of micro-bunches. The length and the transverse dimension of this bunch train are comparable to the pulse width and the spot waist of the laser pulses, respectively. The micro-bunches move at the phase velocity (equation (2)) of the beat wave. As the electron bunches displace, an electrostatic dipole field builds up. In the 1D limit, this field, E_{di} [V m^{-1}], increases linearly over time reaching a maximum dipole field of, from [31]

$$\hat{E}_{di} = \alpha \frac{\omega_p^2}{c\omega} v_\phi \tau, \qquad (3)$$

where the normalized dipole field $\hat{E}_{di} = eE_{di}[\text{V m}^{-1}]/(mc\omega)$, α is the fraction of the trapped electrons, ω_p is the local plasma frequency, ω is the laser frequency, and τ is the pulse duration. Note that, as equation (3) does not depend on a_0, longer laser pulses for a given total pulse energy (sufficient for trapping to occur) would be an advantage in obtaining a high conversion efficiency [31]. However, very long pulses reduce the resolution, and therefore, in this case, they should preferably collide obliquely to minimise the overlap volume. After the two counter-propagating laser pulses have passed each other the PM potential barrier vanishes and the electron micro-bunches merge to form a single macro-bunch, which begins to oscillate at ω_p.

This procedure for generating a dipole has been confirmed by 1D PIC simulations (figure 1) in a 200 μm long domain with a $\Delta x = 0.05$ μm mesh size. The time step is $\Delta t = 1.6 \times 10^{-16}$ s and the number of simulation particles 1000/cell. For the first ~ 0.48 ps, the two laser pulses only generate a wake field (the alternating diagonal lines). The laser pulses collide after 0.48 ps and produce a strong dipole field (the central bright spots). The oscillating dipole field does not decay in 1D (because radiative energy is not lost) after the pulses have left the overlap region.

The length of the macro-bunch (i.e. the dipole) is proportional to the duration of the laser pulse. However, when the laser pulses are very long, single dipole generation becomes unstable: micro-bunches begin to oscillate out of phase and produce modes with a high wavenumber. The 1D PIC simulations suggest that when the duration of the laser pulses is ≈ 30 fs, for a plasma density of 10^{18} cm^{-3}, the electrons move as a stable single dipole.

The Langmuir wave (wake field) and the dipole oscillation can be differentiated by the phase relation between the oscillating elements. In the wake, electrons that oscillate at ω_p have a periodic phase distribution, whereas all of the electrons inside the dipole oscillate in-phase, so that the $k = 0$ mode is dominant (figure 1(b)). In the time domain, all measured oscillations at different positions inside the dipole show peaks at the plasma frequency. Hence, the radiation from the plasma dipole may be quasi-narrowband.

The plasma frequency depends on the local position for inhomogeneous densities. By making the laser pulses collide at different positions and measuring the radiation frequency it

is possible to quantify the local plasma density distribution. Sweeping the collision position enables an arbitrary, non-uniform, plasma density profile to be reconstructed, as will be shown using 2D PIC simulations in the next section.

Two-dimensional simulations of reconstruction of the non-uniform plasma density

In this section, we investigate radiation from the dipole using two-dimensional (2D) PIC simulations and reconstruction of non-uniform plasma densities. Various density profiles are loaded into the simulations; by intersecting the laser pulses at different positions, we can reconstruct the original density profiles. Profiles used in the simulations include linear and nonlinear density profiles increasing from zero with different slopes, and a non-monotonic density gradient.

The density diagnostic entails two steps; induction of the PDO, which emits the radiation, and detection of the radiation from which the local density is inferred. The dipole is created by two counter-propagating laser pulses with wavelengths of 800 nm and 780 nm, respectively. The wavelengths and laser amplitude can be optimized, depending on the plasma density and the normalised laser field amplitude a_0 is chosen to be in the range $0.1 \leqslant a_0 \leqslant 0.3$, which is weakly relativistic. Smaller amplitudes can be used, but then the dipole-generation mechanism is due to a nonlinear current [32], rather than trapped particles. To obtain a much stronger radiation field and therefore a high signal-to-noise ratio, we have chosen the trapped-particle scheme. The effects of obliquely-launched pulses will also be studied as it increases the radiation efficiency and resolution.

A simulation is set up (figure 2) to determine the density by probing the emitted radiation. The mesh size in each direction is $\Delta x = 0.05\ \mu$m and $\Delta y = 0.2\ \mu$m, which resolves the laser wavelength roughly by 20 and 5, respectively. Note that the finer resolution in the x-direction is justified, since the laser pulse propagates predominantly in this direction. Furthermore, the highly anisotropic mesh helps reduce numerical dispersion. The time step is $\Delta t = 1.6 \times 10^{-16}$ s, which marginally satisfies the CFL (Courant–Friedrichs–Lewy) condition. The number of simulation particles is 10/cell. The simulation domain has dimensions of 400 μm × 400 μm. When the dipole is generated at the midpoint of the density gradient it starts emitting radiation at ω_p (right column of figure 2(a)). For demonstration purposes, two virtual probes are placed inside the simulation domain: Probe 1 at the dipole centre, and Probe 2 in vacuum. The laser pulses are directed from two sides at $(x, y) = (0\ \mu$m, 340 μm) and $(x, y) = (400\ \mu$m, 340 μm) and propagate obliquely to collide at $y = 250\ \mu m$. The values of E_x and B_z at probe 1, recorded as a function of time (figure 2(b)), show that the dipole field has non-zero curl electric field components $(\nabla \times E \neq 0)$, that are responsible for the radiation. Laser pulses reach the focal position at $t \approx 7.31$ ps; the plot of $E_x, B_z - t$ (figure 2(b)) confirms this. Values of the normalized electric and magnetic fields recorded by probe 2 located in vacuum at $(x, y) = (200\ \mu$m, 60 μm) (figure 2(c)) coincide both in magnitude and in phase. This result clearly shows that

these fields correspond to the radiation field. The frequency distributions of both signals and their fast Fourier transformed pair show that the radiation frequency from probe 2 corresponds to the oscillation frequency of the dipole (figure 2(d)).

This verifies the fundamental principle of measurement of the local density in non-uniform plasma. We now show how to reconstruct the plasma density by sweeping the collision position of the laser pulses, and probing the radiation. For the same linear gradient of the plasma density used in figure 2, the laser pulses are made to counter-propagate and collide at different positions along the gradient (figure 3(a)). Emitted radiation is detected by the virtual probe located outside the plasma (figure 3(b)). The spectra of the radiation (figure 3(b)) demonstrate that the position of the peaks depends on the collision position of the laser pulses. By converting the peak frequency to density from $\omega_p = \sqrt{e^2 n/(m\epsilon_0)}$, where ϵ_0 is the permittivity of vacuum, the density profile can be reconstructed (figure 3(c)).

Changing the laser pulse entrance is not always possible in practical systems. The laser-launching window is usually fixed, and therefore the launching angle and timing should be adjusted to vary the collision position. Though it is not the subject of this paper, we note that the conversion efficiency of the driving pulse energy to the radiation energy can be increased by oblique collision of the pulses; equation (3) indicates that the dipole field strength can be increased by increasing the pulse duration for a given total pulse energy, where the long pulses should collide obliquely to generate a dipole with spatially limited dimension [31], to detect local densities. However, use of obliquely oriented laser beams for dipole generation has a disadvantage. When the collision angle is too large, lasers tend to drive electrons in the transverse direction in addition to the longitudinal direction. As a result, the location of the dipole may become uncertain, possibly leading to less accurate measurements.

We have conducted systematic simulations of the density reconstruction by obliquely colliding laser pulses (figure 4) by changing the launching angle. Figure 4(b) shows the reconstruction of a linear density profile from pulse collisions with small (15°) and large (30°) angles. As expected, the reconstruction is much better at smaller angles (15°) than for a larger angle (30°); the data points are closer to the density profile and the error bars are smaller for the small angle case. In figure 4(c), we assume that the laser entrance window is located at a fixed position far from the plasma (figure 4(a)). The laser launching position is located so that the collision angle of the pulses is smaller than 15°, i.e. motivated by the results of figure 4(b). For various linear density gradients of plasmas, the original density is accurately reproduced.

The density profiles in real plasma systems are usually nonlinear. In principle, there is no particular reason why the PDO method should not work for nonlinear density profiles. To confirm this, we have performed simulations for two nonlinear profiles: a cosine function and an exponential function. These curves are typical solutions of plasma diffusion found in many bounded and unbounded plasma systems. As shown in figure 5, the dipole method still reproduces the
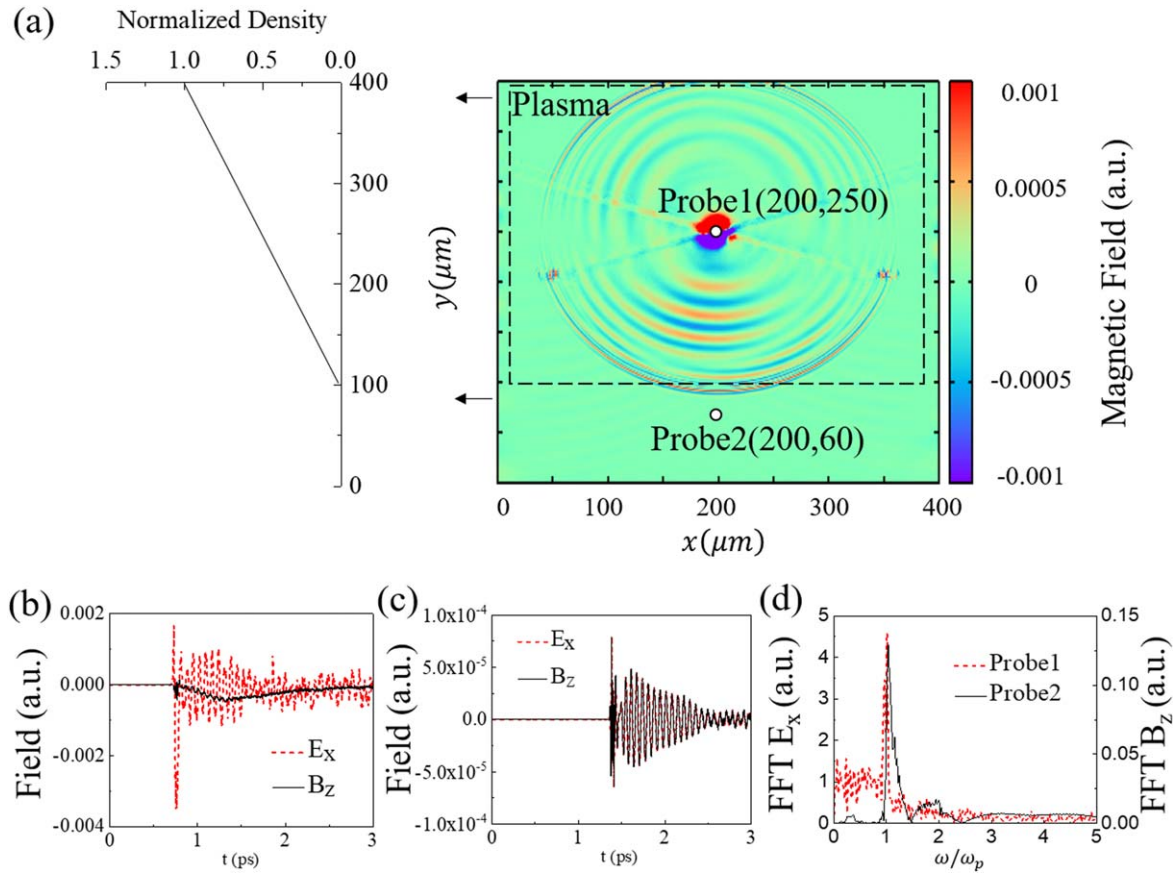
Figure 2. (a) Set-up of a linear plasma density (gradient in the $+y$ direction) and the radiation pattern when the laser pulses collide at $y = 250$ μ**m**. The normalised density increases linearly from zero at $y = 100$ μ**m** to $n/n_0 = 1$ at $y = 400$ μ**m**, where $n_0 = 4.96 \times 10^{18}$ **cm**$^{-3}$. The simulation domain has dimensions of 400 μ**m** $\times$ 400 μ**m**. Broken-line box indicates the plasma region and all other regions are vacuum. The wavelengths of the laser pulses are 800 nm and 780 nm, pulse duration is 30 fs and spot size is 5 μ**m**. Normalized peak amplitude (electric field) of the pulses is $a_0 = eE/(mc\omega) = 0.3$ for both pulses. The ions are assumed to be immobile. Temporal signal of the fields E_x and B_z acquired from the virtual probes located at (b) the dipole centre (probe 1) and (c) in the vacuum side (probe 2). (d) FFT of the probe data inside the dipole (probe 1) and in vacuum (probe 2). Frequency is normalized by plasma frequency ω_p at the collision position.

original density profiles with a high precision (small error-bars). However, the measured density deviates significantly from the exact values in the low density region of the exponential density. This error could have several different numerical and physical origins, such as too few simulation particles at low densities, which would increase the numerical inaccuracy, or the dipole dimension is small compared with the wavelength of the dipole radiation, which can distort the oscillation frequency. Neither of these hypotheses have been confirmed yet.

Measurement of a deep density trough is not possible by the PDO method, because PDOs in a trough emit radiation at a frequency that is below the cut-off of the ambient more dense regions of the plasma. In figure 6, we reconstruct the density profile with a density trough over 200 μm $< y <$ 300 μm, but which is otherwise monotonic. The density is reconstructed with reasonably good error bars over the monotonic parts (100 μm $< y <$ 200 μm and 300 μm $< y <$ 400 μm), but not in the trough of the density profile. The densities deduced from the radiation frequencies over this region are consistently close to the value at $y = 200$ μm, which corresponds to the

peak of the density bump on the left side of the trough. This is because the low frequency portion of the emitted wave is cut off by the density bump, and only spectral components with $\omega > \omega_{p,200\,\mu m}$, which is the plasma frequency at $y = 200$ μm (i.e. where the density peaks), can propagate through the density bump. The intensity of the radiation that originates within the density trough is smaller than at other positions by orders of magnitude, which is because most of the radiation energy is trapped by the cut-off of the ambient plasma. The spectral power decreases as ω increases, so the spectrum of the radiation that passes through the density bump peaks at the cut-off frequency $\omega_{p,200\mu m}$. This is the reason why the density over the trough is measured to be flat as at $n_{200\mu m}$. Complementary methods to measure the density dip are discussed later.

Discussion

We have performed 2D PIC simulations in a parameter regime relevant to laser-plasma interactions, where the plasma density is on the order of 10^{18} cm^{-3}, and the driving
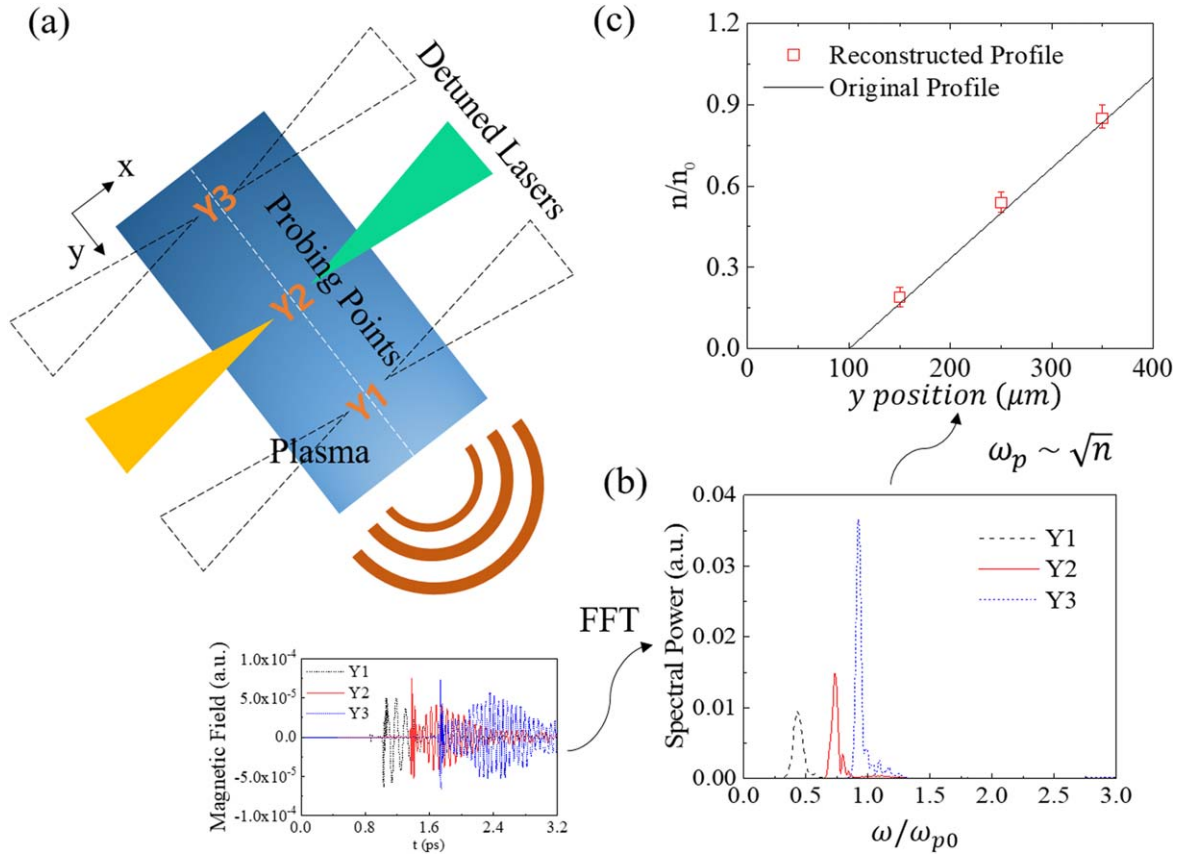
Figure 3. Counter-propagating laser pulses and demonstrative density measurements (a) schematic diagram of counter-propagating lasers to induce the radiation. Magnetic field versus time of probe readings (lower graph) at $Y_{1,2,3} = 150\ \mu m$, $250\ \mu m$, $350\ \mu m$. (b) Power spectra of the data in frequency domain obtained from FFT. Frequency is normalized by the plasma frequency of n_0. (c) Density reconstruction. Vertical axis indicates density normalized by $n_0 = 4.96 \times 10^{18}\ cm^{-3}$; horizontal axis is the direction of the density gradient (y-direction of the simulation domain). The error bars represent the spectral full bandwidth of the radiation at half-maximum (FWHM).

wavelength is approximately 1 μm. However, these parameters can be readily scaled for use in diagnostics of other plasmas, e.g. fusion plasma in a Tokamak. The important scaling parameters are the ratio of the dipole displacement to the wavelength of the radiation (R) and the product of the pulse amplitude and the duration (D). The ratio R is proportional to the electric current of the dipole oscillation and hence it determines the radiation intensity. The parameter D determines the threshold for the electron trapping [31]. The displacement is estimated to be $v_\phi \tau \sim \frac{\omega_p}{2\omega} c\tau$ [31]. Then the ratio of this to the vacuum wavelength of the radiation is

$$R \sim \frac{\omega_p^2}{4\pi\omega}\tau. \tag{4}$$

The parameter D is, in a normalized form

$$D = a_0 \omega \tau. \tag{5}$$

The relation between the power and the normalized vector potential is, assuming the spot size at the diffraction limit (i.e. $\sigma \sim \lambda$), roughly

$$a_0 \sim \frac{\sqrt{P[W]}}{3 \times 10^5}. $$

For a 30 fs laser with $\lambda \sim 1\ \mu$m and $a_0 \sim 0.1$ in plasma of $n \sim 10^{18}\ cm^{-3}$, which are the parameters used in this paper,

$R \sim 10^{-3}$ and $D \sim 5$. When we assume a fusion plasma of density $10^{14}\ cm^{-3}$ probed by lasers with $\lambda \simeq 10\ \mu$m, the required pulse duration and the power to obtain the similar levels of R and D are 10 ps and megawatt, which can be readily obtained using modern CO_2 lasers. When we consider an even lower density plasma, e.g. $n \sim 10^{12}\ cm^{-3}$, which is typical in low temperature plasmas such as in ICPs or in the edge of Tokamaks, the required power of the driving pulse is even more relaxed.

Our method depends on how long the undriven plasma oscillation (i.e. the PDO) is sustained without being disrupted by collisional events between the electrons and neutrals or electrons and ions. The same issue can arise in other cross-beam schemes (used for the purposes other than the diagnostics) such as the plasma photonic crystal [36] or plasma holography [37]. In low density plasma, the collision between electrons and neutrals can be significant. The electron-neutral collision frequency, given by $\nu_{en}[s^{-1}] \sim 2 \times 10^{-7} n_n[cm^{-3}](T_e[eV])^{1/2}$ [38], however, is usually much lower than the plasma frequency ($f_p = \omega_p/c$); for typical low temperature plasmas obtained from breakdown of gases with a few Pascal pressure, $n_n \sim 10^{13}\ cm^{-3}$ and $T_e \sim 1$ eV, leading to $\nu_{en} \sim 1$ MHz, while the plasma frequency is in the range of a few GHz for $n_e \sim 10^{12}\ cm^{-3}$. At the edge of Tokamak plasma, the temperature is of order 1 keV, but the neutral density is very low;
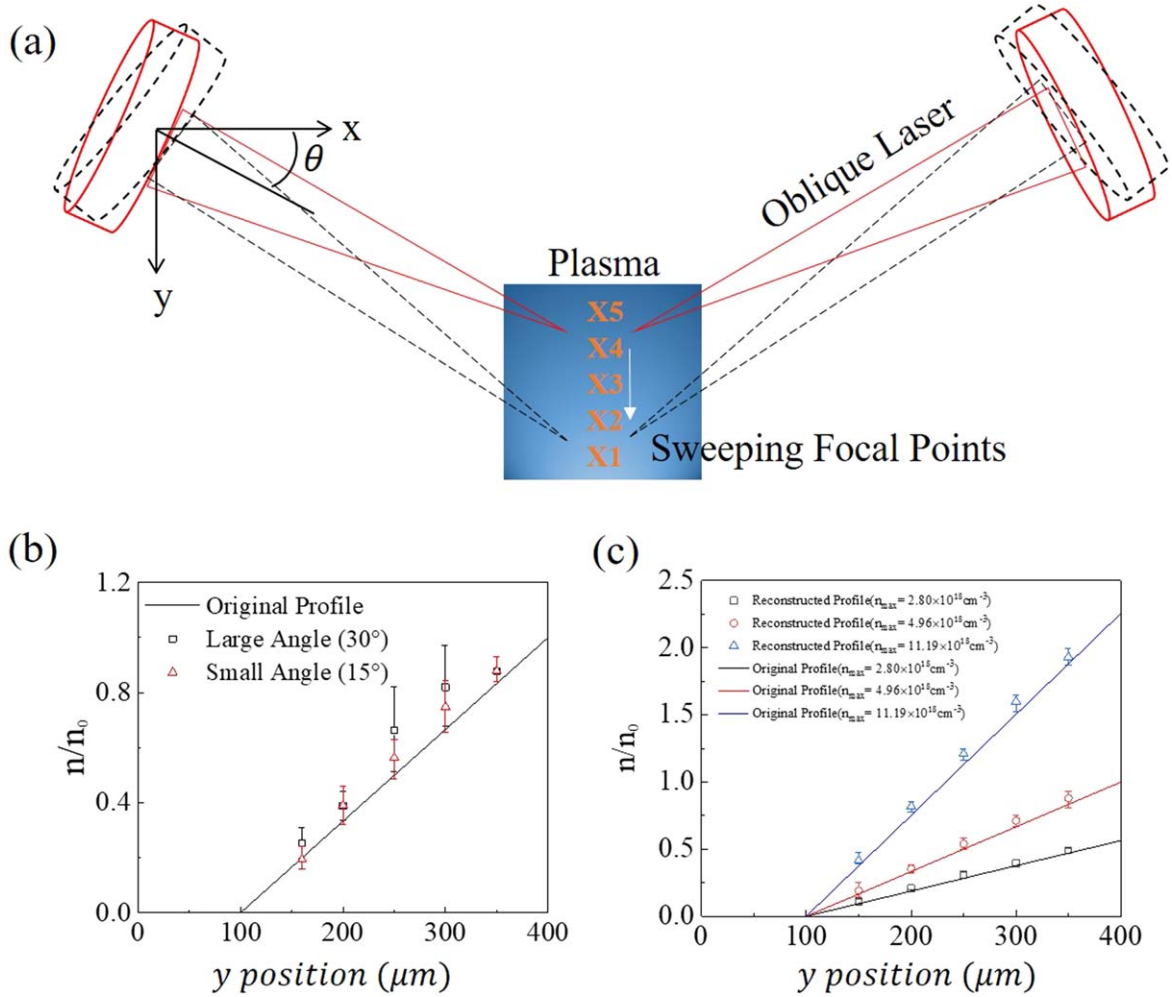
Figure 4. Obliquely propagating laser pulses and demonstrative density measurements (a) schematic diagram of obliquely propagating lasers to induce the radiation. (b) Reconstructed density profile for small (15°) and large (30°) collision angles and (c) density reconstruction of three different gradients by sweeping shot angles of the pulses at fixed launching positions located far from the plasma. $n_{\max}$ in the legend represents the maximum density at $y = 400\,\mu$m. Vertical axes in (b) and (c) represent the density normalized by $n_0 = 4.96 \times 10^{18}$ cm^{-3}; horizontal axes are the y-position along the gradient. Laser wavelengths are $\lambda_1 = 800$ nm, $\lambda_2 = 780$ nm and normalized peak amplitude $a_0 = 0.3$.

even close to the diverter target where the neutral density has a maximum, $n_n < 10^{14}$ cm^{-3}, for which ν_{en} is lower than the plasma frequency $f_p \sim 1$ GHz. Hence, the electron-neutral collisions may not critically affect the PDO emission in most plasma sources.

The electron-ion collisions in high-density, laser-produced plasma can disrupt the PDO oscillation. From the electron-ion collision frequency given by ν_{ei} [s^{-1}] $\simeq 3 \times 10^{-5} n_e$ [cm^{-3}]$(T_e$[eV])$^{-3/2}$ [38], for $n_e \sim 10^{18}$ cm^{-3} (used throughout this paper), T_e should be larger than 10 eV to ensure ν_{ei} below 10 percent of f_p. The condition $T_e > 10$ eV is satisfied in many laser-plasma interactions. Furthermore, the electron bunch of the plasma dipole is intrinsically thermal because the dipole is generated by electron trapping induced from the wave-breaking, which usually results in heating of the electrons. From [31], it is observed that the thermal velocity of the dipole bunch is of order $\beta = v/c \sim 0.01$, corresponding to $T_e \sim 50$ eV, which is sufficiently high for ν_{ei} to be negligible. Although our PIC code does not capture collisional

phenomena, the results are still valid because electron-ion collisions are negligible at such high temperatures.

The intensity decay of the PDO emission over distance is pertinent to determining the required sensitivity of the detectors. It was demonstrated in [31] that the emission from a PDO obeys the pattern of two-dimensional dipole radiation. In a three dimensional system, the field strength of the dipole radiation can be roughly estimated as

$$E \sim E_0 \frac{\sigma_{di}}{r},$$

where σ_{di} is the transverse width of the dipole and E_0 is the field strength at the transverse edge of the dipole, i.e. at $r \sim \sigma_{di}$. Note that σ_{di} is roughly the same as the spot size σ of the laser pulse. Usually σ is comparable to the plasma wavelength $\lambda_p = 2\pi c/\omega_p$. When the emitted field is measured at $r \sim N\lambda_p$, then $E \sim E_0/N$. In the laser-produced plasmas used throughout this paper, $N \sim 100$ and $E_0 \sim 1$ GV m^{-1}, leading to $E \sim 10$ MV m^{-1} at the measurement point, which is sufficiently strong to be detected. When we make the same
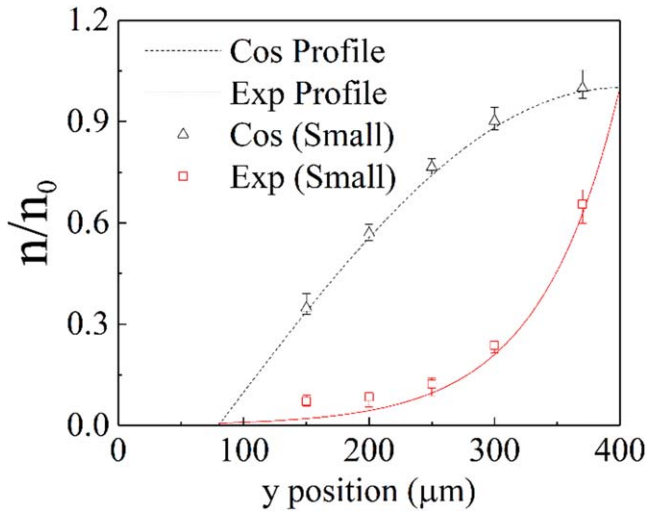
Figure 5. Reconstruction of the nonlinear density profiles, one is cosine (dotted, triangles) and the other is exponential (solid, rectangles). The exact profiles are $n/n_0 = \cos[\pi(y - 400)/640]$, and $n/n_0 = \exp[(y - 400)/100]$. The laser pulses made small angle collisions (i.e. under 15°). $n_0 = 4.96 \times 10^{18}$ cm^{-3} and the laser parameters are the same as in figure 4.
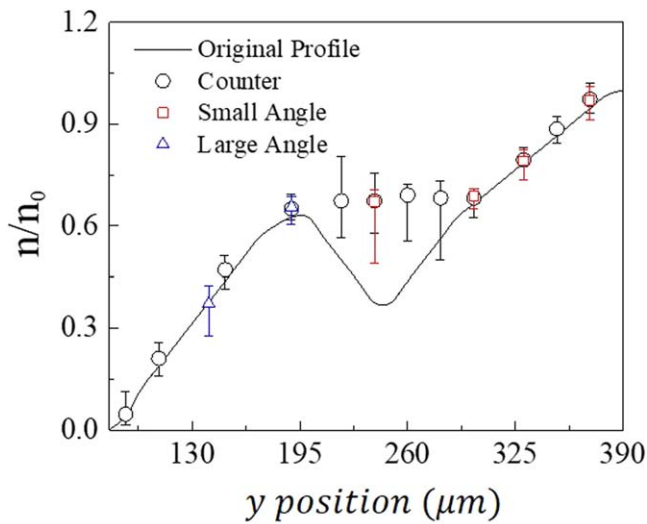
Figure 6. Reconstruction of the non-monotonically-increasing density profiles. Vertical axis: reconstructed value normalized by the maximum value $n_0 = 4.96 \times 10^{18}$ cm^{-3}. The normalized peak amplitude of the laser field is $a_0 = 0.3$. The simulation domain has the same dimension as in figures 3 and 4. The wavelengths of the laser pulses are 800 and 780 nm, the pulse duration is 30 fs and spot size is 5 μm.

estimate for the nuclear fusion or low temperature plasma, $\lambda_p \sim 1$ mm ($n_e \sim 10^{14}$ cm^{-3}) and $N \sim 1000$ for detection at 1 m. Noting that as $E_0 \propto n_e$ and $E_0 \sim 10^5$ V m^{-1}, the field determined at 1 m from the dipole is of order a few hundred V m^{-1}, which is still very strong and readily measurable.

A finite electron temperature T_e will affect the generation of dipoles. The important parameter in thermal plasma is the relative strength of the dipole field compared with the thermal noise. We have conducted 1D simulations for $T_e = 1$ keV and 10 keV (figure 7), which are typical parameters used in this

paper. These result in a very strong dipole oscillation (stronger than the thermal noise) when driven by pulse with $a_0 = 0.1$ and $T_e = 1$ keV. Temperatures in a magnetically confined fusion plasma, such as in ITER-class tokamaks, can reach ~10 keV, so the higher temperature case has also been simulated (figure 7(b)). Since the thermal noise is usually numerically enhanced in PIC simulations, because a simulation particle represents many real particles, the signal-to-noise ratio could be grossly underestimated in the simulations. As the ratio of the simulation particles to the real particles increases, the numerical-thermal noise decreases significantly, which enables the dipole oscillation to be clearly visible (red line in figure 7(b)). At higher driving pulse intensity (blue line in figure 7(b)), the dipole oscillation becomes even more prominent, implying that the dipole method can also be used to measure the density of core plasma in a Tokamak. A huge number of simulation particles must be used to yield a realistic noise level, which results in the requirement of significant computational resources for 2D radiation simulations, which remains the subject of future study.

The oscillation frequency of the dipole in thermal plasma is not different to the cold plasma frequency, because the $k = 0$ mode is dominant for the dipole, as described in Section II, therefore the thermal effect in the Bohm-Gross dispersion relation is negligible. In contrast, the dipole oscillation frequency can be significantly affected by a magnetic field (and its direction). The magnetic dependence of the dipole method can also be exploited to detect the magnetic field in highly magnetized plasma, such as fusion plasma.

Throughout this paper, we have considered the cases where the spot sizes (σ) and pulse widths ($c\tau$) are much smaller than the scale length (L_{grad}) of the density gradient. Under that condition, i.e.

$$\sigma, c\tau \ll L_{grad} = \frac{n}{\nabla n}, \tag{6}$$

the local plasma dipole is found to be generated stably and to yield quasi-narrowband radiation, enabling the measurement of the local plasma density. As long as condition (6) is met, the density of the local region of the plasma, where the induced PDO is located, can be considered quasi-homogeneous and the PDO oscillates effectively in a homogeneous plasma. However, if the density variation of plasmas is large compared to the laser spot size or the pulse length, the oscillation modes determined from the local density within laser spot are mixed and produce uncertainty in the oscillation frequency of the PDO, reducing the monochromaticity of the radiation. From a series of simulations, we find that the spectral broadening of PDO emission becomes very severe when σ (*or* $c\tau$)/$L_{grad} > 0.1$ (corresponding to a density variation of 10% over the dimension of the dipole), making the method significantly less useful for diagnostics. An exact expression for the maximum measurable density gradient can be obtained only after the robustness of the dipole oscillation on a steep density gradient is fully studied.

As shown in figure 6, the PDO method has a weak point in measuring non-monotonic density profiles. This problem
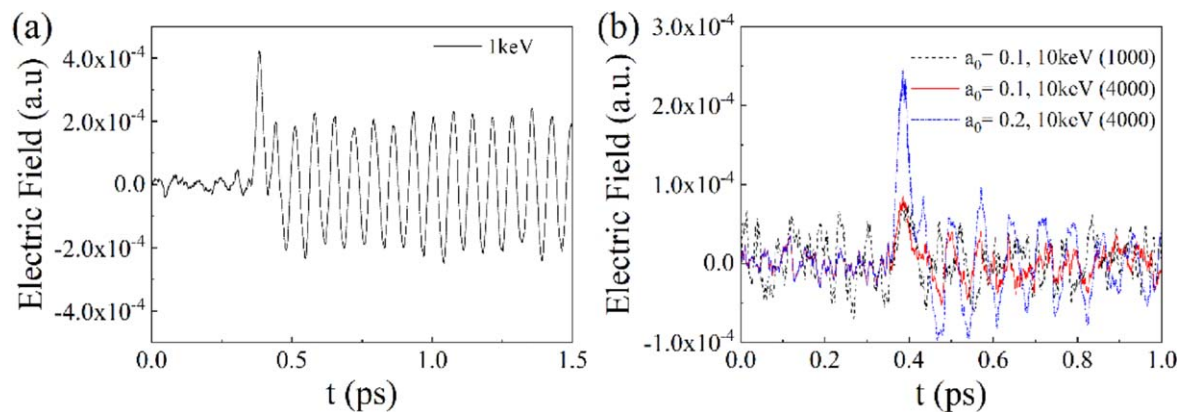
Figure 7. Generation of the dipole oscillation in thermal plasmas with (a) $T_e = 1\,keV$ and (b) 10 keV. The normalized amplitude of the driving laser pulses is $a_0 = 0.1$ for 1 keV and $a_0 = 0.1$ and 0.2 for 10 keV. The simulations were repeated increasing the number of simulation particles per cell, n_s, to reach the quasi-saturation of the numerical noise. In (b), n_s is denoted in the parentheses of the legend. The numerical-thermal noise decreases significantly for the larger n_s.

can be partially resolved by exploiting the emission of second harmonic radiation, which can propagate through the density bump better than the fundamental harmonic, though more intense laser pulses are required to drive a nonlinear oscillation of the PDO. Generation of the second harmonic has only been observed infrequently in our simulations. The origins of the second harmonic generation are thought to be the merger of two plasmons [39] (i.e. by the collision of the wake plasma waves) or the nonlinear current generated by collision of asymmetric laser pulses [40], but the exact condition for second harmonic emission remains obscure. Also, the chirped pulse Raman backscatter [14] can complement the PDO method, because both methods share the same experimental configuration of colliding laser pulses, and can be easily combined as a unified diagnostic method.

Summary

We have presented simulations of a new diagnostic method for probing the local plasma density and reconstructing non-uniform density profiles. The concept exploits the fact that the local PDO oscillates at the local plasma frequency, and emits EM radiation that has a similar frequency. Hence, the plasma density can be determined from the measured radiation frequency. A novel aspect is the method of generating the local PDO can be achieved by colliding two detuned electromagnetic pulses at any desired position, head-on or obliquely. The overlap region of the colliding pulses can be kept very small compared with the scale length of the plasma density variation, so that a precise measurement of the local plasma density can be obtained, whereas conventional methods such as interferometry or spectroscopy yield only line integrals. By sweeping the collision position of the pulses by changing the launching angle, a non-uniform density can be reconstructed in 2D PIC simulations. We have evaluated this method only for laser-produced plasmas, but the simple scaling indicates that it can be applied to diagnostics of fusion-plasma and low-temperature, collisional plasma for plasma processing, using CO_2 lasers. The stable dipole oscillation of the PDO for highly thermal plasmas is demonstrated using 1D simulations. This result strongly implies also that the suggested method can be used as a diagnostic of high-temperature plasma.

ORCID iDs

M S Hur https://orcid.org/0000-0002-6661-1467

References

[1] Hutchinson I H 2002 *Principles of Plasma Diagnostics* (Cambridge: Cambridge University Press) (https://doi.org/10.1017/CBO9780511613630)
[2] Equipe TFR 1978 Tokamak plasma diagnostics *Nucl. Fusion* **18** 647
[3] Donné A J H, Barth C J and Weisen H 2008 Chapter 4: laser-aided plasma diagnostics *Fusion Sci. Technol.* **53:2** 397–430
[4] Li W M *et al* 2019 Bench test of phase measurement on dispersion interferometer for EAST *Rev. Sci. Instrum.* **90** 026105
[5] Park H K 2019 Newly uncovered physics of MHD instabilities using 2D electron cyclotron emission imaging system in toroidal plasmas *Adv. Phys.* X **4** 1633956

[6] Laviron C, Donné A J H, Manso M E and Sanchez J 1996 Reflectometry techniques for density profile measurements on fusion plasmas *Plasma Phys. Control. Fusion* **38–7** 905–36

[7] Tokuzawa T *et al* 2018 Microwave frequency comb Doppler reflectometer applying fast digital data acquisition system in LHD *Rev. Sci. Instrum.* **89** 10H118

[8] Mazzucato E 2014 Plasma Reflectometry *Electromagnetic Waves for Thermonuclear Fusion Research* (Singapore: World Scientific) ch 7, pp 123–62

[9] Morales R B, Hacquin S, Heuraux S and Sabot R 2017 New density profile reconstruction methods in X-mode reflectometry *Rev. Sci. Instrum.* **88** 043503

[10] Kang T, Kwon K B, Cho M H, Kim Y K, Hur M S, Park H K and Lee W 2018 Envelope-PIC hybrid method for the simulation of microwave reflectometry *IEEE Trans. Plasma Sci.* **46** 577

[11] Borghesi M *et al* 1996 Characterization of laser plasmas for interaction studies: progress in time-resolved density mapping *Phys. Rev.* E **54** 6769–73

[12] Quevedo H J, McCormick M, Wisher M, Bengtson R D and Ditmire T 2016 Simultaneous streak and frame interferometry for electron density measurements of laser produced plasmas *Rev. Sci. Instrum.* **87** 013107

[13] David D R *et al* 1994 Measurement of laser-plasma electron density with a soft x-ray laser deflectometer *Science* **265** 514–7

[14] Vieux G, Ersfeld B, Farmer J P, Hur M S, Issac R C and Jaroszynski D A 2013 Plasma density measurements using chirped pulse broad-band Raman amplification *Appl. Phys. Lett.* **103** 121106

[15] Nagornyi D A, Nagornyi A G and Voznyi V I 2005 A microwave interferometer for steady-state plasma density measurements *Instrum Exp. Tech.* **48** 225

[16] Torrisi G *et al* 2016 Microwave frequency sweep interferometer for plasma density measurements in ECR ion sources: Design and preliminary results *Rev. Sci. Instrum.* **87** 02B909

[17] Kim T H *et al* 2013 Plasma characteristics of inductively coupled plasma using dual-frequency antennas *Japan. J. Appl. Phys.* **52** 05EA02

[18] Park S, Choe W, Moon S Y and Yoo S J 2018 Electron characterization in weakly ionized collisional plasmas: from principles to techniques *Adv. Phys.* X **4** 1526114

[19] Jang J, Park S, Park J Y and Choe W 2018 Tomography-based spatial uniformity diagnostics for meter-sized plasmas *Plasma Source Sci. Tech.* **27** 10LT01

[20] Langmuir I and Compton K T 1931 Electrical discharges in gases:II. Fundamental phenomena in electrical discharges *Rev. Mod. Phys.* **3** 191

[21] Cherrington B E 1982 The use of Langmuir probes for plasma diagnostics *Rev. Plasma Chem. Plasma Process.* **2** 113–40

[22] Chen F F 2003 *Langmuir Probe Diagnostics EE* (Los Angeles: University of California)

[23] Ussenov Y A E, Wahl V, Marvi Z, Ramazanov T S and Kersten H 2019 Langmuir probe measurements in nanodust containing argon-acetylene plasmas *Vacuum* **166** 15–25

[24] Siegfried H G and Redmer R 2009 X-ray Thomson scattering in high energy density plasmas *Rev. Mod. Phys.* **81** 1625

[25] Kozlowski P M, Crowley B J B, Gericke D O, Regan S P and Gregori G 2016 Theory of Thomson scattering in inhomogeneous media *Sci. Rep.* **6** 24283

[26] Segre S E 1999 A review of plasma polarimetry—theory and methods *Plasma Phys. Control. Fusion* **41** R57

[27] Song H S, Cho M H, Kim Y K, Kang T Y, Suk H and Hur M S 2016 Measurement of local density and magnetic field of a magnetized plasma using Raman scattering from a focused laser pulse *Plasma Phys. Control. Fusion* **58** 025006

[28] Cho M H, Kim Y K and Hur M S 2014 Measuring the magnetic field of a magnetized plasma using Raman scattering *Appl. Phys. Lett.* **104** 141107

[29] Jang H, Hur M S, Lee J M, Cho M H, Namkung W and Suk H 2008 A method to measure the electron temperature and density of a laser-produced plasma by Raman scattering *Appl. Phys. Lett.* **93** 071506

[30] Ciocarlan C *et al* 2013 The role of the gas/plasma plume and self-focusing in a gas-filled capillary discharge waveguide for high-power laser-plasma applications *Phys. Plasmas* **20** 093108

[31] Kwon K B, Kang T Y, Song H S, Kim Y K, Ersfeld B, Jaroszynski D A and Hur M S 2018 High-energy, short-duration bursts of coherent terahertz radiation from an embedded plasma dipole *Sci. Rep.* **8** 145

[32] Cho M H, Kim Y-K, Suk H, Ersfeld B, Jaroszynski D A and Hur M S 2015 Strong terahertz emission from electromagnetic diffusion near cutoff in plasma *New J. Phys.* **17** 043045

[33] Hur M S and Suk H 2011 Numerical study of 1.1 GeV electron acceleration over a-few-millimeter-long plasma with a tapered density *Phys. Plasmas* **18** 033102

[34] Yang X *et al* 2015 Chirped pulse Raman amplification in warm plasma towards controlling saturation *Sci. Rep.* **5** 13333

[35] Vieux G *et al* 2017 An ultra-high gain and efficient amplifier based on Raman amplification in plasma *Sci. Rep.* **7** 2399

[36] Lehmann G and Spatschek K H 2016 Transient plasma photonic crystals for high-power lasers *Phys. Rev. Lett.* **116** 225002

[37] Dodin I Y and Fisch N J 2002 Storing, retrieving, and processing optical information by Raman backscattering in plasmas *Phys. Rev. Lett.* **88** 165001

[38] Sprangle P, Peñano J R, Hafizi B and Kapetanakos C A 2004 Ultrashort laser pulses and electromagnetic pulse generation in air and on dielectric surfaces *Phys. Rev.* E **69** 066415

[39] Teubner U *et al* 1997 Observation of VUV radiation at wavelengths in the ω_p- and $2\omega_\mathrm{p}$-wavelength range emitted from femtosecond laser-plasmas *Opt. Commun.* **144** 217–21

[40] Timofeev I V, Annenkov V V and Volchok E P 2017 Generation of high-field narrowband terahertz radiation by counterpropagating plasma wakefields *Phys. Plasmas* **24** 103106